Title

Resonance Hyper-Raman Scattering from CdSe and CdS Nanocrystals

Journal

The Journal of Physical Chemistry C, 123(26)

ISSN

1932-7447

Authors

Tan, Rui
Kelley, David F
Kelley, Anne Myers

Publication Date

2019-07-05

DOI

10.1021/acs.jpcc.9b04645

Resonance Hyper-Raman Scattering from CdSe and CdS Nanocrystals

Rui Tan, David F. Kelley and Anne Myers Kelley*

Chemistry and Chemical Biology, University of California, Merced, 5200 North Lake Rd., Merced, CA 95343; amkelley@ucmerced.edu

Abstract

Resonance hyper-Raman spectra are reported for zincblende and wurtzite CdSe quantum dots (QDs), CdS quantum dots, and CdSe/CdS tetrapods in toluene solution using 808-824 nm excitation. All structures show both Stokes and anti-Stokes fundamental scattering and overtone scattering in the CdS or CdSe longitudinal optical phonon, but the hyper-Rayleigh scattering is much stronger relative to the hyper-Raman in the tetrapods than in the QDs. This may reflect a larger relative contribution of nonresonant and preresonant hyper-Rayleigh scattering in the tetrapods, as suggested by model calculations, or it may be related to the more nearly centrosymmetric structure of the QDs, rendering the hyper-Rayleigh scattering less strongly allowed. The hyper-Raman spectra are similar for wurtzite and zincblende CdSe QDs and for zincblende CdSe QDs with different surface ligands.

Introduction

Hyper-Raman and hyper-Rayleigh scattering (Figure 1) are the two-photon excited analogs of ordinary Raman and Rayleigh scattering.[1,2] Two incident photons in the red to near-IR are coherently destroyed and a scattered photon in the near-UV to blue is produced having twice the frequency of the incident light (hyper-Rayleigh), plus or minus one or more ground-state vibrational quanta (hyper-Raman). When the two-photon energy falls within an optical absorption band, the dominant intermediate states in the process are excitonic transitions that are both two-photon and one-photon allowed.[1] Accordingly, hyper-Rayleigh scattering is nominally forbidden within the dipole approximation for strictly centrosymmetric systems, because only the "u" symmetry transitions are one-photon allowed and only the "g" symmetry transitions are two-photon allowed. Hyper-Raman scattering in such systems is allowed only through vibronic coupling mechanisms and is generally expected to be weak.[3] We have previously demonstrated this in conjugated organic molecules; resonance hyper-Raman scattering is strong in highly asymmetric, donor-acceptor substituted "push-pull" molecules, while in symmetrically substituted, nominally centrosymmetric systems the hyper-Raman scattering is observable but very weak, presumably allowed through ground-state conformational distortions and/or transiently asymmetric solvation.[4-6]

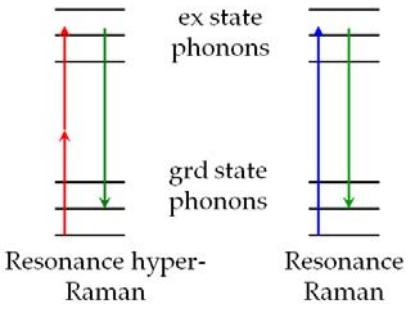

Figure 1. Resonance Raman and hyper-Raman scattering.

Here we extend these studies to II-VI semiconductor nanocrystals. There have been some prior studies of both electronically nonresonant[7-11] and resonant[12-15] hyper-Rayleigh scattering in II-VI quantum dots (QDs). To our knowledge hyper-Raman spectra have been reported for

only one II-VI nanocrystal system: resonant hyper-Rayleigh and hyper-Raman spectra of CdS QDs grown in a silicate glass were reported over the range 920 to 720 nm, with the maximum intensity obtained near the lowest one-photon absorption maximum.[16,17]

We report the resonance hyper-Rayleigh and hyper-Raman spectra of CdSe QDs having both wurtzite and zincblende crystal structures, different surface ligands, and produced by different synthetic routes, as well as zincblende CdS QDs and tetrapods having a zincblende CdSe core and CdS arms. Our initial interest was in comparing structures that should be nearly centrosymmetric (QDs) with one that is highly noncentrosymmetric (tetrapods, having a tetrahedral arrangement of CdS arms around the CdSe core). Hyper-Rayleigh scattering should be strictly forbidden in a completely centrosymmetric QD within the electric dipole approximation, while hyper-Raman scattering can still be allowed for phonons that break the center of symmetry. We do not expect hyper-Rayleigh scattering to be strictly forbidden in QDs, however, because the underlying crystal structure, whether zincblende or wurtzite, lacks an inversion center. Furthermore, a roughly spherical structure composed of a finite number of atoms will rarely have exact inversion symmetry, and the distribution of ligands on the surface is also likely to have some asymmetry. We expect this comparison to provide some insight into the extent of electron-hole asymmetry in nominally spherical QDs, as well as the influence of crystal structure and ligation on that asymmetry. The hyper-Rayleigh and hyper-Raman intensities are also strongly influenced by electronic resonance effects, which are different for all three structures. Computational methods previously developed to simulate resonance hyper-Raman spectra of organic molecules[5,6] and resonance Raman spectra of semiconductor QDs[18-21]

are modified to calculate resonance hyper-Rayleigh and hyper-Raman spectra of CdSe QDs for comparison with our experimental results.

Experimental methods

Six samples were examined: wurtzite CdSe QDs (wzCdSe), zincblende CdSe QDs synthesized using elemental Se (zb1CdSe), zincblende CdSe QDs synthesized using SeO_2 (zb2CdSe), those particles subsequently ligand exchanged with oleylamine (zb3CdSe), CdS QDs, and CdSe/CdS tetrapods. The synthetic details are described and TEM images are shown in the Supporting Information. The four CdSe samples were chosen to compare the effects of crystal structure (zincblende versus wurtzite), of the same core with different surface ligands (zb2CdSe and zb3CdSe), and of synthesis in a different redox environment (zb1CdSe and zb2CdSe). All four CdSe samples have similar absorption spectra (Figure 2) with the lowest excitonic absorption at 573-580 nm. Both the wurtzite QDs and the zincblende ones ligated with oleylamine exhibit a significantly smaller splitting between the two lowest excitonic transitions than do the other zincblende samples as reported previously.[22] The CdS QDs and the tetrapods also have similar absorption spectra to one another (Figure 3) with the onset of a CdS-localized excitonic absorption near 450 nm, while the tetrapods additionally have weaker transitions involving the CdSe core near 600 nm. Using the sizing curves of Jasieniak *et al.*, the CdSe QDs have a diameter of about 3.8 nm and the concentrations of the samples used for the hyper-Rayleigh and hyper-Raman experiments are about 2.0 μM. According to ref. 23, the CdS QDs have a diameter of about 5.3 nm and the concentrations of the samples in the nonlinear scattering experiments are about 0.6 μM. The molar concentrations of the tetrapods, having considerably greater per-particle

volumes, were considerably lower than for the QDs but the concentrations were not determined quantitatively.

All samples were prepared in toluene at optical densities near 1.0 per cm at the two-photon resonant wavelength. The hyper-Raman/hyper-Rayleigh measurements were carried out using the apparatus and methods described previously.[6] A Spectra-Physics Tsunami picosecond Ti:sapphire laser produced 805-825 nm, 1-2 ps, 5-7 nJ pulses at 82 MHz. The laser was focused into a fluorescence cuvette containing the sample with a 20 mm focal length lens. The nonlinear scattering was collected at 90° with a fused silica lens, focused through IR-blocking filters into a 0.5-meter single spectrograph, and detected with a liquid nitrogen cooled CCD detector. Linear Raman spectra were obtained as described previously[18] with the frequency doubled Ti:sapphire laser used as the excitation source.

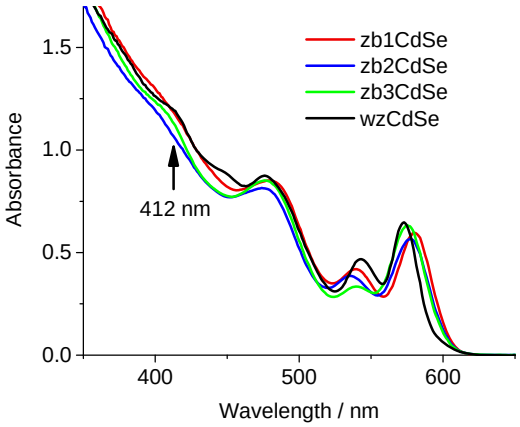

Figure 2. Absorption spectra of the four CdSe QDs. The two-photon excitation wavelength used for the hyper-Raman experiments is indicated.

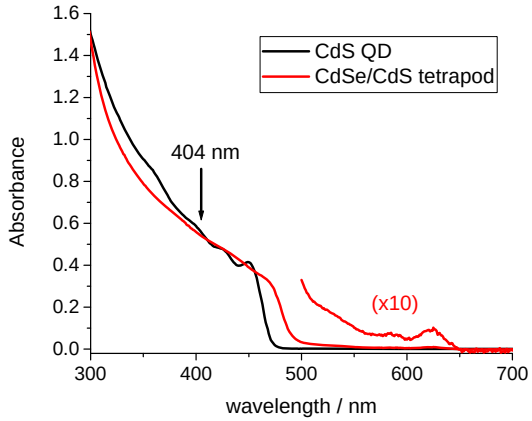

Figure 3. Absorption spectra of the CdS QDs and CdSe/CdS tetrapods. The two-photon excitation wavelength used for the hyper-Raman experiments is indicated.

Results

Figure 4 compares the hyper-Raman spectra of the four different CdSe QDs excited at 824 nm. All four samples show a strong hyper-Rayleigh peak, weaker Stokes and anti-Stokes transitions in the longitudinal optical (LO) phonon near 205 cm^{-1}, and a hint of the first Stokes overtone of the LO phonon. The relative intensities of the hyper-Rayleigh and hyper-Raman peaks are similar for all four samples. The toluene solvent makes a significant contribution to the hyper-Rayleigh scattering as indicated in the figure legend, and this is accounted for in the hyper-Rayleigh to hyper-Raman intensity ratios quoted below.

Figure 5 compares the hyper-Raman spectra of the CdS QDs and CdSe/CdS tetrapods excited at 808 nm. Both the CdS QD and the tetrapod samples exhibit hyper-Raman scattering in the CdS LO phonon near 300 cm^{-1}. In the QDs the hyper-Raman scattering is nearly as strong as the hyper-Rayleigh, with both the anti-Stokes and Stokes LO fundamentals being observed in addition to the Stokes LO overtone. Higher overtones, if present, are masked by the greatly increased noise from the underlying two-photon excited fluorescence at larger Raman shifts. The tetrapods show both the anti-Stokes and Stokes CdS LO fundamentals as well as the $\Delta v = 2$, 3, and 4 overtones in this mode, but the hyper-Raman scattering is much weaker than the hyper-Rayleigh. The failure to observe the CdSe LO phonon when exciting on two-photon resonance with CdS-localized excitons is consistent with previous studies using linear resonance Raman spectroscopy[19] and with the estimated CdS to CdSe volume ratio of about 30 in the tetrapods.

Figures 6 and 7 show the linear resonance Raman spectra of the same samples excited at the two-photon wavelength. The solvent was chloroform rather than toluene to avoid interference from solvent Raman lines. All of the spectra show the fundamental of the CdS or CdSe LO

phonon as well as the first overtone. The overtone to fundamental intensity ratio is roughly comparable for all of the structures, slightly weaker for the CdSe QDs.

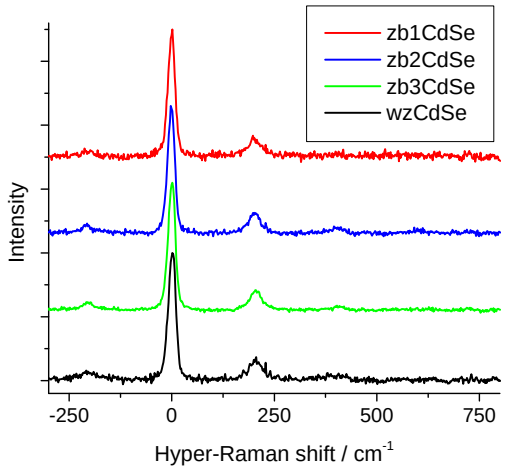

Figure 4. Hyper-Raman spectra of the samples in Figure 2, excited at 824 nm, scaled to constant hyper-Rayleigh intensity. Weak backgrounds have been subtracted. The toluene solvent contributes about 40% of the hyper-Rayleigh intensity.

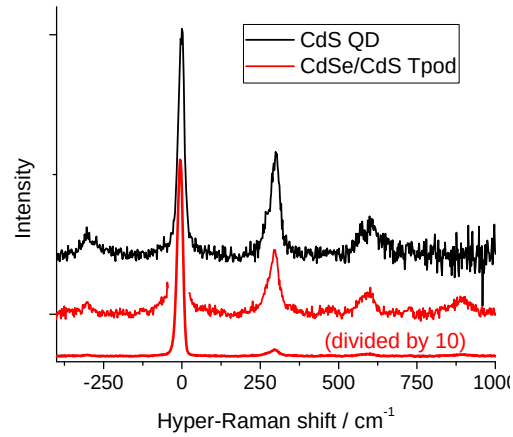

Figure 5. Hyper-Raman spectra of the samples in Figure 3, excited at 808 nm. The toluene solvent contributes about 20% of the hyper-Rayleigh intensity in the CdS QDs but makes a negligible contribution in the tetrapods. Fluorescence backgrounds have been subtracted.

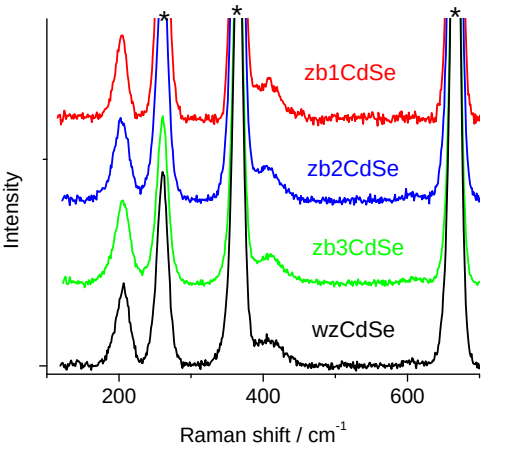

Figure 6. Linear Raman spectra of the samples in Figure 2, excited at 412 nm, in chloroform solvent. Asterisks label solvent peaks. Weak fluorescence backgrounds have been subtracted.

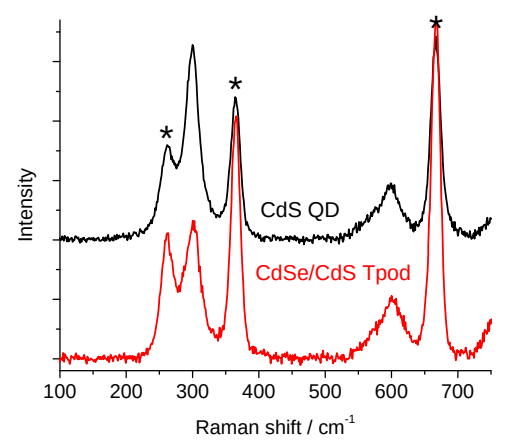

Figure 7. Linear Raman spectra of the samples in Figure 3, excited at 404 nm, in chloroform solvent. Asterisks mark solvent peaks. Fluorescence backgrounds have been subtracted.

Discussion

Here we discuss possible origins for the large differences in the hyper-Raman to hyper-Rayleigh intensity ratio among the structures studied. The hyper-Rayleigh to LO fundamental integrated intensity ratio, corrected for the solvent contribution to the hyper-Rayleigh line, is about 14 for the tetrapods, about 2 for the CdSe QDs, and about 1 for the CdS QDs.

We begin by noting that the hyper-Rayleigh scattering intensity can, in general, be partitioned into a part arising from an ensemble of uncorrelated molecules scattering independently and a part resulting from interferences between the fields generated by correlated pairs of molecules.[24] The latter part is usually assumed to be negligible in dilute solution where the positions and orientations of the scatterers are uncorrelated, and we assume that this is the case in the analysis that follows. However, in a structure such as a tetrapod, the correlated positions and orientations of the four arms will show up in the hyper-Rayleigh intensity even if the electronic excitations are localized to a single arm. This is not the case for hyper-Raman scattering as long as the phonons that are excited are localized to a single arm of the tetrapod. See ref. 25 for further discussion in the context of molecules.

For spontaneous emission from the v = 0 vibrational level, *e.g.* relaxed fluorescence from a cold sample, the intensities of the 0→v vibrational transitions should obey the Poisson distribution, $I_v \propto e^{-S}\frac{S^v}{v!}$ where S is the Huang-Rhys parameter. The same pattern should hold for resonance Raman or resonance hyper-Raman scattering if the excitation is resonant with an isolated origin transition of a single electronic state. However, in room-temperature ensembles of colloidal semiconductor quantum dots an isolated electronic origin transition is never seen, and multiple vibronic or excitonic states contribute as intermediate states in the scattering process. Interferences among those contributions result in different and not always obviously predictable intensity patterns,[26,27] but usually the higher v transitions are relatively weaker

because the effectively faster electronic dephasing has a larger effect on damping the intensities of the higher overtones. This holds for both linear Raman and hyper-Raman when there are no one-photon resonances in the excitation step,[6] except that different excitonic states may contribute with different amplitudes in the two processes.

Figures 4-7 show that the first overtone to fundamental intensity ratios for all of the structures are somewhat larger in the linear Raman spectra than in the hyper-Raman. While we might reasonably expect similar overtone to fundamental intensity ratios in hyper-Raman and linear Raman at the same total excitation energy because the same excitonic states are resonant, different near-resonant excitonic states having different Huang-Rhys parameters may contribute differently in two-photon excitation compared with one-photon excitation. Although there are many reasons why the overtone to fundamental intensity ratio cannot be used alone as a quantitative measure of the Huang-Rhys parameter,[28] both the linear Raman and hyper-Raman data are consistent with effective (averaged over multiple excitonic states) Huang-Rhys parameters in the S = 0.4 - 0.7 range. The hyper-Rayleigh intensity is also qualitatively consistent with the hyper-Raman intensities for the CdSe and CdS QDs. However, the very strong hyper-Rayleigh scattering from the tetrapods is harder to rationalize; the very small v = 1 to v = 0 intensity ratio suggests a very small Huang-Rhys parameter for the resonant excitonic states, which is inconsistent with the observation of comparatively strong 2- and 3-quantum transitions in Figure 4. Note that in Figure 4, the hyper-Raman part of the spectrum looks very similar for the tetrapods and the CdS QDs, but the hyper-Rayleigh peak is much stronger in the tetrapods.

It is tempting to ascribe the large hyper-Rayleigh intensity in the tetrapods to the complete lack of inversion symmetry of this structure compared with the approximate spherical symmetry of the QDs. In a tetrahedral structure, there should be many excitonic states that are both one-photon and two-photon allowed and the hyper-Rayleigh and hyper-Raman scattering should be

fully symmetry allowed. In a nearly spherical QD, there should be no excitonic states that are strongly allowed in both one-photon and two-photon absorption and the hyper-Rayleigh scattering should be very weak, while the hyper-Raman scattering can still be symmetry allowed through vibronic coupling to a phonon whose envelope function breaks the spherical symmetry. The two-photon absorption spectra of CdSe QDs are very different from the one-photon spectra,[29] providing some support for this hypothesis. However, numerous experiments on both wurtzite and zincblende II-VI QDs show large ground-state dipole moments,[30,31] indicating a strong breaking of inversion symmetry and suggesting that hyper-Rayleigh scattering should be symmetry allowed in all of the structures studied.

(Hyper-) Rayleigh scattering should be much less sensitive to rapid electronic dephasing than (hyper-) Raman scattering, and nonresonant and preresonant transitions also contribute much more strongly to (hyper-) Rayleigh than to (hyper-) Raman. The CdS QDs have the smallest hyper-Rayleigh to hyper-Raman intensity ratio and are also the structures excited at the lowest energy above the absorption onset (~3000 cm^{-1}, compared with 8000-10000 cm^{-1} for the CdSe-based structures). We have carried out calculations of the hyper-Rayleigh and hyper-Raman relative intensities for a simple model of the two-photon resonant excitonic transitions, making different assumptions about the electronic linewidths (dephasing rates) to demonstrate the effect on the calculated hyper-Raman to hyper-Rayleigh intensities. The model is similar to that used in ref. 19, where we approximate the low-energy part of the CdS QD absorption spectrum by a sum of 10 excitonic transitions having comparable cross-sections. Calculations were carried out for a Huang-Rhys parameter of S = 0.4 (S = 0.2 - 0.5 for the LO phonons on resonance with lower-lying excitonic states of CdSe and ZnSe QDs[32]) and three different choices for the excitonic homogeneous linewidth--200, 400, and 600 cm^{-1}. Figure 8 shows the resulting absorption spectrum, hyper-Rayleigh intensity, and hyper-Raman to hyper-Rayleigh ratio. The absorption

spectrum can be fit equally well over a wide range of linewidths and the hyper-Rayleigh intensities excited near 400 nm (25,000 cm^{-1}) vary by less than a factor of two over this range of linewidths. However, the fundamental hyper-Raman to hyper-Rayleigh intensity ratio varies from 0.02 to 0.47 over this range. Additionally, at any choice of homogeneous width, the hyper-Raman to hyper-Rayleigh ratio is greatly reduced as the two-photon excitation energy is tuned to the blue of the lowest exciton. The very large hyper-Rayleigh to hyper-Raman intensity ratio in the tetrapods may be caused at least in part by contributions from a large number of resonant excitonic states and fast electronic dephasing at these high excess energies.

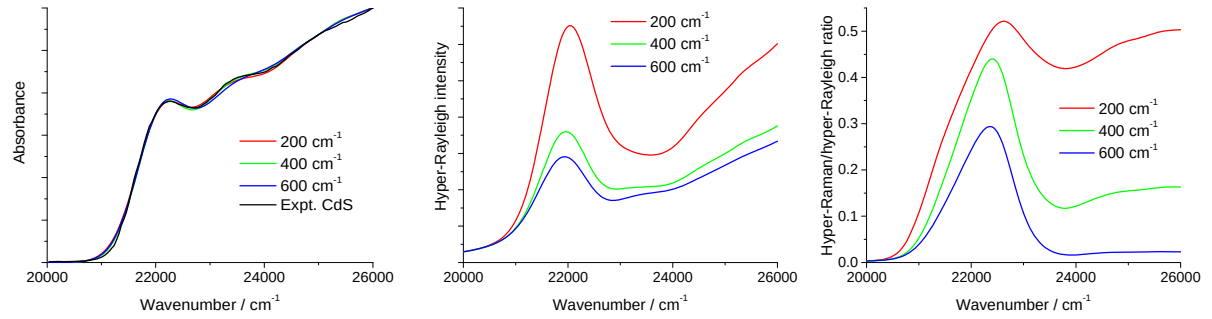

Figure 8. Left: experimental absorption spectrum of CdS QDs and calculated spectra modeled using the excitonic linewidths given. The four plots are almost superimposable. Middle: calculated hyper-Rayleigh cross-sections for the three linewidths. Right: calculated fundamental hyper-Raman to hyper-Rayleigh intensity ratio for the three linewidths.

Finally, we note that the tetrapods are relatively large structures, spanning a range of about 40 nm from tip to tip, while the QDs have diameters of 4-5 nm. The dipole approximation for the radiation-matter interaction is probably good for the QDs but may break down for the much larger tetrapods. Thus, contributions to the scattering intensities from higher-order terms in the multipole expansion of the radiation-matter interaction may have to be considered.

Conclusions

These preliminary studies suggest a variety of avenues for further study. Ongoing and future experiments will further probe the effects of overall symmetry, crystal structure, and resonance on the hyper-Rayleigh and hyper-Raman spectra. The effects of crystal structure and ligands on the absolute hyper-Rayleigh intensity (first hyperpolarizability) are being probed as a proxy for the overall electronic asymmetry of the structure. Comparison of CdSe/CdS tetrapods with CdSe/CdS core/shell QDs having the same core and comparable CdSe to CdS volume ratios will help elucidate the relative importance of the overall shape (centrosymmetric or not) and the underlying crystal structure. The relative contributions of resonant and near-resonant states to the hyper-Raman and hyper-Rayleigh scattering can be elucidated through a combination of varying the sizes of CdSe and CdS QDs and tuning the laser excitation wavelength. Finally, measurements of the hyper-Rayleigh and hyper-Raman depolarization ratios could provide insight into the extent of delocalization of the electronic and vibrational excitations.[25]

Acknowledgements

This work was supported by NSF grant CHE-150680.

Supporting information

Details of the synthetic methods; TEM images; calculations of hyper-Rayleigh and hyper-Raman intensities. This material is available free of charge via the Internet at http://pubs.acs.org.

References

(1) Kelley, A. M. Hyper-Raman Scattering by Molecular Vibrations. *Ann. Rev. Phys. Chem.* **2010**, *61*, 41-61.

(2) Ziegler, L. D. Hyper-Raman Spectroscopy. *J. Raman Spectrosc.* **1990**, *21*, 769-779.

(3) Chung, Y. C.; Ziegler, L. D. The Vibronic Theory of Resonance Hyper-Raman Scattering. *J. Chem. Phys.* **1988**, *88*, 7287-7294.

(4) Leng, W.; Bazan, G. C.; Kelley, A. M. Solvent Effects on Resonance Raman and Hyper-Raman Scatterings for a Centrosymmetric Distyrylbenzene and Relationship to Two-Photon Absorption. *J. Chem. Phys.* **2009**, *130*, 044501.

(5) Shoute, L. C. T.; Bartholomew, G. P.; Bazan, G. C.; Kelley, A. M. Resonance Hyper-Raman Excitation Profiles of a Donor-Acceptor Substituted Distyrylbenzene: One-Photon and Two-Photon States. *J. Chem. Phys.* **2005**, *122*, 184508.

(6) Shoute, L. C. T.; Blanchard-Desce, M.; Kelley, A. M. Resonance Hyper-Raman Excitation Profiles and Two-Photon States of a Donor-Acceptor Substituted Polyene. *J. Phys. Chem. A* **2005**, *109*, 10503-10511.

(7) Santos, B. S.; Pereira, G. A. L.; Petrov, D. V.; de Mello Donega, C. First Hyperpolarizability of CdS Nanoparticles Studied by Hyper-Rayleigh Scattering. *Opt. Commun.* **2000**, *178*, 187-192.

(8) Zhang, Y.; Wang, X.; Ma, M.; Fu, D.; Gu, N.; Lu, Z.; Xu, J.; Xu, L.; Chen, K. Size Dependence of Second-Order Optical Nonlinearity of CdS Nanoparticles Studied by Hyper-Rayleigh Scattering. *J. Colloid Interface Sci.* **2003**, *266*, 377-381.

(9) Zhang, Y.; Ma, M.; Wang, X.; Fu, D.; Gu, N.; Liu, J.; Lu, Z.; Ma, Y.; Xu, L.; Chen, K. First-Order Hyperpolarizability of ZnS Nanocrystal Quantum Dots Studied by Hyper-Rayleigh Scattering. *J. Phys. Chem. Solids* **2002**, *63*, 2115-2118.

(10) Zhang, Y.; Wang, X.; Fu, D.; Cheng, J.; Shen, Y.; Liu, J.; Lu, Z. Second-Order Optical Nonlinearity Study of CdS Nanoparticles via Hyper-Rayleigh Scattering. *J. Phys. Chem. Solids* **2001**, *62*, 903-906.

(11) Petrov, D. V.; Santos, B. S.; Pereira, G. A. L.; de Mello Donegá, C. Size and Band-Gap Dependences of the First Hyperpolarizability of $Cd_xZn_{1-x}S$ Nanocrystals. *J. Phys. Chem. B* **2002**, *106*, 5325-5334.

(12) Eilon, M. J.; Mokari, T.; Banin, U. Surface Exchange Effect on Hyper Rayleigh Scattering in CdSe Nanocrystals. *J. Phys. Chem. B* **2001**, *105*, 12726-12731.

(13) Jacobsohn, M.; Banin, U. Size Dependence of Second Harmonic Generation in CdSe Nanocrystal Quantum Dots. *J. Phys. Chem. B.* **2000**, *104*, 1-5.

(14) Landes, C.; Braun, M.; El-Sayed, M. A. The Effect of Surface Adsorption on the Hyper-Rayleigh Scattering of Large and Small CdSe Nanoparticles. *Chem. Phys. Lett.* **2002**, *363*, 465-470.

(15) Winter, S.; Zielinski, M.; Chauvat, D.; Zyss, J.; Oron, D. The Second Order Nonlinear Susceptibility of Quantum Confined Semiconductors—a Single Dot Study. *J. Phys. Chem. C* **2011**, *115*, 4558-4563.

(16) Baranov, A. V.; Inoue, K.; Toba, K.; Yamanaka, A.; Petrov, V. I.; Fedorov, A. V. Resonant Hyper-Raman and Second-Harmonic Scattering in a CdS Quantum-Dot System. *Phys. Rev. B* **1996**, *53*, R1721-R1724.

(17) Inoue, K.; Baranov, A. V.; Yamanaka, A. Resonant Hyper-Raman Scattering in Semiconductor Quantum Dots. *Physica B* **1996**, *219&220*, 508-510.

(18) Baker, J. A.; Kelley, D. F.; Kelley, A. M. Resonance Raman and Photoluminescence Excitation Profiles and Excited-State Dynamics in CdSe Nanocrystals. *J. Chem. Phys.* **2013**, *139*, 024702.

(19) Gong, K.; Kelley, D. F.; Kelley, A. M. Resonance Raman Excitation Profiles of CdS in Pure CdS and CdSe/CdS Core/Shell Quantum Dots: CdS-Localized Excitons. *J. Chem. Phys.* **2017**, *147*, 224702.

(20) Lin, C.; Gong, K.; Kelley, D. F.; Kelley, A. M. Size Dependent Exciton-Phonon Coupling in CdSe Nanocrystals through Resonance Raman Excitation Profile Analysis. *J. Phys. Chem. C* **2015**, *119*, 7491-7498.

(21) Lin, C.; Gong, K.; Kelley, D. F.; Kelley, A. M. Electron-Phonon Coupling in CdSe/CdS Core-Shell Quantum Dots. *ACS Nano* **2015**, *9*, 8131-8141.

(22) Chen, O.; Yang, Y.; Wang, T.; Wu, H.; Niu, C.; Yang, J.; Cao, Y. C. Surface-Functionalization-Dependent Optical Properties of II-VI Semiconductor Nanocrystals. *J. Am. Chem. Soc.* **2011**, *133*, 17504-17512.

(23) Yu, W. W.; Qu, L.; Guo, W.; Peng, X. Experimental Determination of the Extinction Coefficient of CdTe, CdSe, and CdS Nanocrystals. *Chem. Mat.* **2003**, *15*, 2854-2860.

(24) Bersohn, R.; Pao, Y.-H.; Frisch, H. L. Double-Quantum Light Scattering by Molecules. *J. Chem. Phys.* **1966**, *45*, 3184-3198.

(25) Kelley, A. M.; Shoute, L. C. T.; Blanchard-Desce, M.; Bartholomew, G. P.; Bazan, G. C. Resonance Raman, Hyper-Raman, and Hyper-Rayleigh Depolarization Ratios and Symmetry Breaking in Solution. *Mol. Phys.* **2006**, *104*, 1239-1247.

(26) Kelley, A. M. Resonance Raman and Resonance Hyper-Raman Intensities: Structure and Dynamics of Molecular Excited States in Solution. *J. Phys. Chem. A* **2008**, *112*, 11975-11991.

(27) Myers, A. B. Excited Electronic State Properties from Ground-State Resonance Raman Intensities. In *Laser Techniques in Chemistry*; Myers, A. B., Rizzo, T. R., Eds.; Wiley: New York, 1995; pp 325-384.

(28) Kelley, A. M. Resonance Raman Overtone Intensities and Electron-Phonon Coupling Strengths in Semiconductor Nanocrystals. *J. Phys. Chem. A* **2013**, *117*, 6143-6149.

(29) Schmidt, M. E.; Blanton, S. A.; Hines, M. A.; Guyot-Sionnest, P. Size-Dependent Two-Photon Excitation Spectroscopy of CdSe Nanocrystals. *Phys. Rev. B* **1996**, *53*, 12629-12632.

(30) Blanton, S. A.; Leheny, R. L.; Hines, M. A.; Guyot-Sionnest, P. Dielectric Dispersion Measurements of CdSe Nanocrystal Colloids: Observation of a Permanent Dipole Moment. *Phys. Rev. Lett.* **1997**, *79*, 865-868.

(31) Shim, M.; Guyot-Sionnest, P. Permanent Dipole Moment and Charges in Colloidal Semiconductor Quantum Dots. *J. Chem. Phys.* **1999**, *111*, 6955-6964.

(32) Gong, K.; Kelley, D. F.; Kelley, A. M. Resonance Raman Spectroscopy and Electron-Phonon Coupling in Zinc Selenide Quantum Dots. *J. Phys. Chem. C* **2016**, *120*, 29533-29539.

TOC graphic